

Review

Advanced design of catalytically active reaction space
at surfaces for selective catalysisMizuki Tada^{*}, Yasuhiro Iwasawa*Department of Chemistry, Graduate School of Science, The University of Tokyo, Hongo, Bunkyo-ku, Tokyo 113-0033, Japan*

Received 3 January 2007; accepted 15 June 2007

Available online 22 June 2007

Abstract

The recent advanced design of surface reaction spaces for heterogeneous selective catalysis in molecular-nano scales is reviewed, focusing on our recent challenges and also presenting new data. Supported metal complexes on oxide surfaces often exhibit tremendous catalytic properties based on their unique coordination structures created at the surfaces. Novel active reaction spaces can be designed by coordination regulation on central metals, chemical interaction at metal–surface interface, and three-dimensional architectures constructed at surfaces. Such molecularly organized surfaces possess advantageous properties of both homogeneous and heterogeneous catalyst systems and provide great opportunities for the tailor-made design of highly selective catalysis for various kinds of catalytic chemical syntheses.

© 2007 Elsevier B.V. All rights reserved.

Keywords: Supported metal complex; Catalyst surface; Heterogeneous catalyst; Chemical design; Active structure; Molecular imprinting; Chiral self-assembly; Asymmetric catalysis; Oxidative coupling; Selective oxidation; Hydrogenation; Characterization

Contents

1. Introduction: molecularly organized surfaces with supported metal complexes	2702
2. Metal–metal coordination-assisted hydroformylation on oxide-supported Rh dimers	2703
3. Chiral self-dimerized Vanadium Schiff-base complexes on SiO ₂ for asymmetric oxidative coupling of 2-naphthol	2705
4. N-interstitial Re ₁₀ -cluster catalyst on HZSM-5 zeolite for the direct phenol synthesis from benzene and O ₂	2708
5. Molecular-imprinted metal-complex catalysts on oxide surfaces for tailor-made shape-selective catalysis	2710
5.1. General strategy of molecular-imprinted supported metal complexes	2710
5.2. An amine-imprinted Rh monomer catalyst on SiO ₂ and its enzymatic inhibition of alkene hydrogenation	2711
5.3. A molecular-imprinted Rh dimer catalyst on SiO ₂ for highly shape-selective hydrogenation	2713
6. Summary	2715
References	2716

1. Introduction: molecularly organized surfaces with
supported metal complexes

Most artificial chemicals are produced by heterogeneous solid catalysts in industrial processes and the merits of heterogeneous catalysts are not only the separation of catalysts and products from reaction media but also their high durability and catalytic activities derived from the structures of catalytically

active sites at solid surfaces. The relationships between the structure, organized environment, and catalytic property of surface species tell us how to establish a new strategy for the rational design of heterogeneous catalysts. However, solid surfaces are generally complex and heterogeneous, which prevent us from obtaining uniform structures of catalytically active species, resulting in low selectivity.

The attachment of organic and inorganic metal complexes on support surfaces is a promising way to produce molecularly regulated structures of active metal sites at surfaces and various surface metal structures can be arranged by stepwise struc-

^{*} Corresponding author. Tel.: +81 3 5841 4364; fax: +81 3 5841 4364.
E-mail address: mtada@chem.s.u-tokyo.ac.jp (M. Tada).

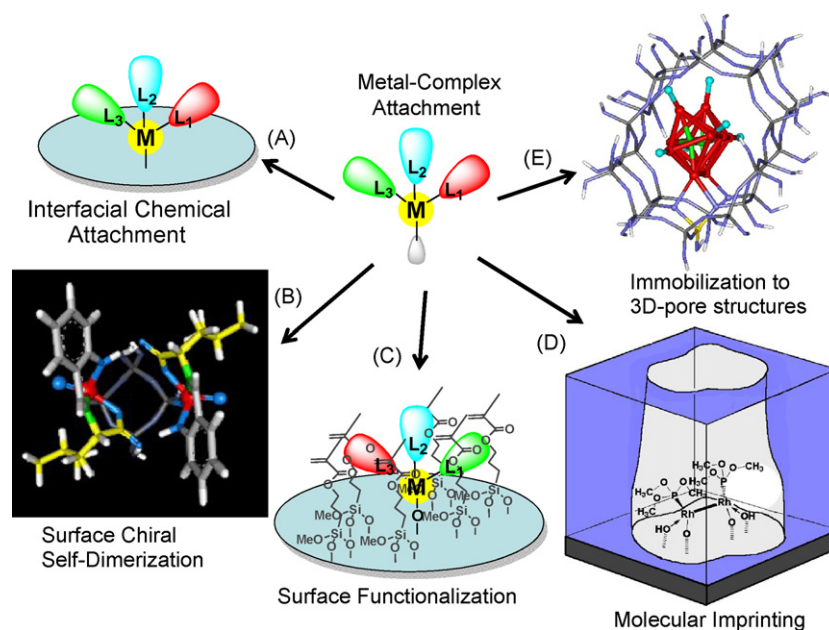


Fig. 1. Strategies for advanced chemical design of catalytically active reaction space on surfaces with supported metal complexes.

tural transformations in a controllable manner [1–11]. There are several types of metal-complex attaching techniques: (a) coordination of metal-complex precursors to immobilized ligands on an organic polymer [12,13], (b) coordination of metal-complexes with functional ligands bound to an oxide surface [2,4], (c) intercalation into clay materials [14], (d) ion exchange into porous materials such as zeolite and mesoporous silica [15], and (e) direct attachment of metal complexes on an oxide surface [3,6,11,16].

There are many review articles on polymer-immobilized metal complexes of the type (a) [12,13,17], which aim to improve separation and recycling of homogeneous metal-complex catalysts with low stability. The type (b) has the similar strategy to the type (a) but using oxide supports without swelling unlike organic polymers by organic solvents [4,17]. This ligand-bound immobilization provides supported metal coordination structures to homogeneous counterparts, and hence similar catalytic activities to those of homogeneous precursor complexes.

On the other hand, the interfacial attachment between metal complexes and support surfaces can produce unique metal coordination different from metal-complex precursors. A chemical bond between a metal-complex precursor and a support surface modifies the reactivity of the supported metal complex, resulting in novel catalytic activity [3,6,11,15,16]. Traditional ion-exchange on zeolites (type (c)) and intercalation to clay materials (type (d)) are also typical ways to introduce metal species onto solid supports although the valences and types of metal precursors are restricted [4,15]. The type (e) involves direct chemical bonds produced by the reaction of metal complexes with hydroxyl groups at oxide surfaces [3,11,16,18]. Many important factors for selective catalysis can be controlled at the interface, such as electronic properties and coordination sphere of the attached metal center, geometry around the active metal center, dispersion, and stability of the attached

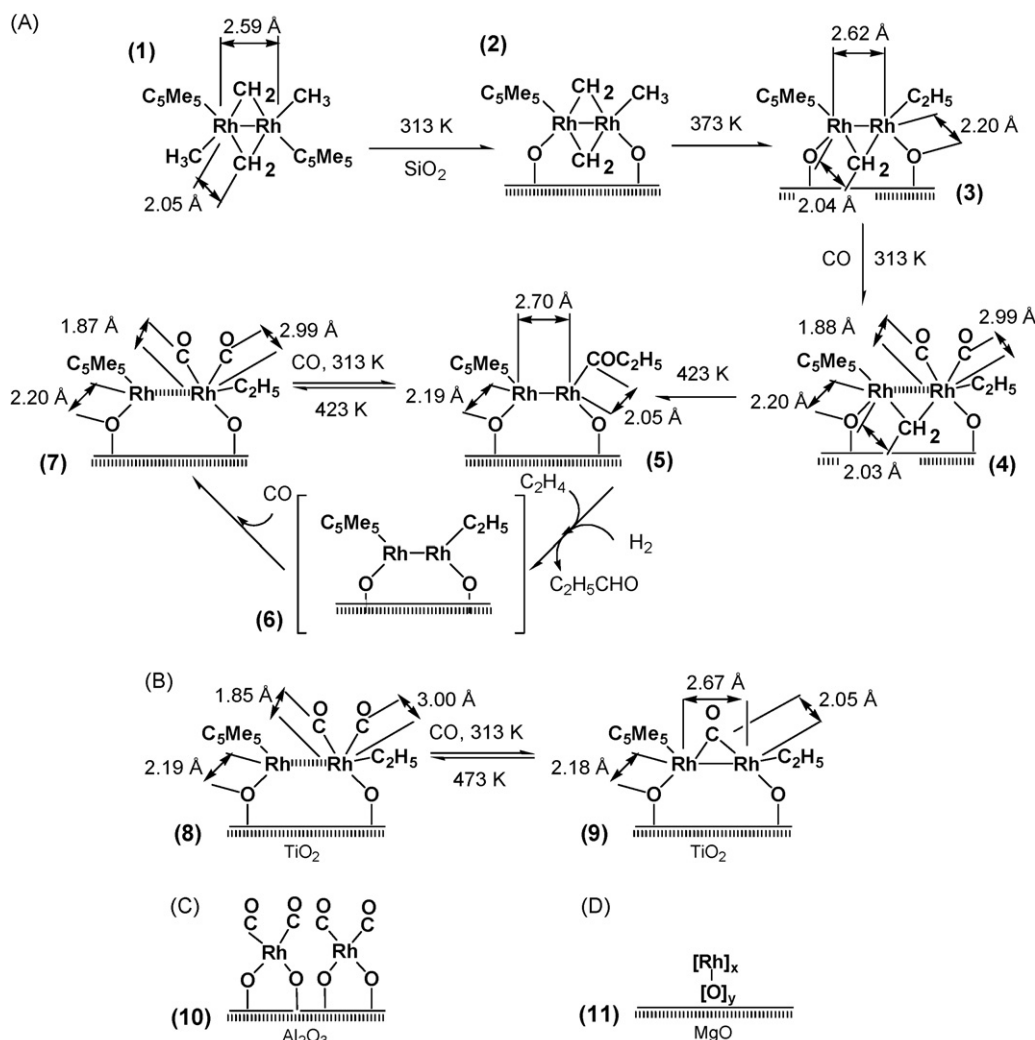
metal sites, etc. Especially, the formation of unsaturated metal sites, which cannot be isolated in homogeneous solution or self-assembled materials, is a key issue for improved catalytic activity [11,19–21].

Recently, we have found several unique phenomena based on the interfacial chemical attachment of metal complexes onto oxide surfaces, (A) interfacial chemical attachment [11,18,19,21], (B) chiral self-dimerization at surfaces [11,20,22], (C) surface functionalization with organic molecules [11,23,24], (D) molecular imprinting [11,23–29] and (E) immobilization to three-dimensional pores [30,31], whose schematic protocols are illustrated in Fig. 1. The interfacial attachment reactions promoted further structural transformations of supported metal complexes and novel selective catalytic processes including asymmetric oxidations can be achieved. In this review, recent examples of the design of supported metal-complex catalysts via interfacial chemical attachment at oxide surfaces are highlighted.

2. Metal–metal coordination-assisted hydroformylation on oxide-supported Rh dimers

Metallic interactions between two metal sites often play a crucial role in catalysis on heterogeneous surfaces and the variation of coordination on metal clusters promotes the bond dissociation of reactant molecules and subsequent bond rearrangement to a desired product. For example, metal particles with an optimum particle size show great activity for hydroformylation. Rh dimers attached directly on oxide surfaces, which are a minimum unit of metal ensembles, showed the unique metal–metal coordination assisted hydroformylation of ethene [16,19,32].

Scheme 1 shows the structural transformations of *trans*-[(RhCp*CH₃)₂(μ-CH₂)₂] (Cp*: pentamethylcyclopentadienyl) dimer (1) on SiO₂, TiO₂, Al₂O₃, and MgO. Each step of the



Scheme 1. Structural transformation of Rh dimers on (A) SiO₂, (B) TiO₂, (C) Al₂O₃, and (D) MgO and their structural changes during ethene hydroformylation.

transformation of the incipient attached Rh species at the surfaces was characterized by FT-IR and EXAFS. A CH₃ group and a μ -CH₂ group reacted to form C₂H₅ on a Rh atom ((3) in Scheme 1(A)). The Rh dimer (3) was exposed to CO to form *gem*-carbonyls (4) and one of the carbonyls inserts into the ethyl ligand to form an acyl ligand (5) by heating at 423 K. Note that the Rh dimer (5) obtained is regarded as a catalytic intermediate for ethene hydroformylation. A Rh dimer species with a Rh–Rh bond was also produced on TiO₂ (9) by using the dimer precursor (1) (Scheme 1(B)). On the other hand, the mononuclear

Rh species (10) was formed on Al₂O₃ and the aggregated Rh species (11) was formed on MgO irrespective of use of the same precursor (1) (Scheme 1(C) and (D)) [32]. The difference of the structures in the Rh species on the oxides may be due to the difference of acidity, lattice parameter, and arrangement of the oxide surfaces.

The catalytic activities and selectivities of those catalysts for ethene hydroformylation are summarized in Table 1. The Rh₂/SiO₂ (5) catalyst showed high activity and selectivity (88.9% for propanal) compared with a conventional impreg-

Table 1
Catalytic activities and selectivities for ethene hydroformylation on Rh dimers attached to SiO₂, TiO₂, Al₂O₃, and MgO at 413 K^a

Catalyst	TOF (total) ^b	TOF (ethene) ^b	TOF (propanal) ^b	Selectivity (%)
Impregnated Rh/SiO ₂	22.8	21.5	1.3	5.6
Rh ₂ /SiO ₂ (5)	36.9	4.1	32.8	88.9
Rh ₂ /TiO ₂ (9)	6.3	6.3	0	0
Rh/Al ₂ O ₃ (10)	6.8	6.8	0	0
Rh _x /MgO (11)	56.0	56.0	0	0

^a Ref. [19]/H₂/C₂H₄ = 1/1/1 (total pressure = 40.0 kPa).

^b TOF was written in 10^{−4} min^{−1}.

nated Rh catalyst, while the Rh dimer on TiO_2 (**9**) did not produce propanal (Table 1). The catalytic activities were highly depended on the CO insertion on the dimeric structures on the oxide surfaces. Thus the transformation of Rh species during the ethene hydroformylation on Rh_2/SiO_2 (**5**) was fully characterized by FT-IR and EXAFS [32]. The acyl ligand is hydrogenated to the corresponding aldehyde product (propanal) as shown in Scheme 1(A). CO molecules coordinate to Rh as geminal dicarbonyls again, accompanied with Rh–Rh bond breaking, leading to two mononuclear sites (**7**) (Scheme 1(A)). The mononuclear species with dicarbonyl groups and an ethyl group (**7**) is transformed to the acyl species (**5**) again at 423 K, accompanied with rebonding of Rh–Rh coordination. The transformation between the structures (**5** and **7**) occurs reversibly. Note that the catalytic ethene hydroformylation on Rh_2/SiO_2 proceeds in conjunction with breaking and reformation of the Rh–Rh bond. This is the first example which clearly illustrates how the metal–metal bonding plays an essential role in solid catalysis on a molecular level. In the Rh_2/SiO_2 catalyst (**5**), one Rh atom with an acyl ligand works as the reaction site, while another Rh atom promotes the Rh reaction site for the CO insertion [32].

Both Rh_2/SiO_2 (**5**) and Rh_2/TiO_2 (**9**) have dimer structures, but their reactivities are very different from each other. The dimeric structure of Rh_2/TiO_2 (**9**) did not act as a catalytic site for ethene hydroformylation, whereas a CO-bridged Rh dimer structure was formed as shown in Scheme 1(B). Further CO treatment brought about dissociation of the Rh–Rh bond to a mononuclear species similar to the case of Rh_2/SiO_2 (**5**), but an acyl species, as a key intermediate for the hydroformylation, was not formed at the reaction temperature. The difference may be caused by electronic and geometric states of the Rh sites. The Rh–Rh bond in Rh_2/SiO_2 (**5**) has such a flexible character which makes CO insertion promoted by the Rh–Rh coordination possible. On Al_2O_3 , metal–support interaction becomes stronger and the Rh species is supported as monomers (**10**), where the formation of the Rh–Rh bond is prohibited. Again, metal–metal assisted CO insertion does not occur on the Al_2O_3 support. On MgO , the Rh dimer is converted to clusters (**11**) during heating the surface Rh dimers. No hydroformylation reaction occurs. On Rh_2/TiO_2 (**9**), $\text{Rh}_2/\text{Al}_2\text{O}_3$ (**10**), and Rh_2/MgO (**11**), the promotion of CO insertion by the adjacent Rh atoms is not observed possibly because the interaction between Rh species and supports are too strong.

Hydroformylation reaction of alkenes is known to proceed on mono-metal sites like mononuclear metal complexes in homogeneous systems. However, mono-metal sites are generally disadvantageous because of the necessity to eliminate a part of intimate ligands to form an unsaturated site on the metal atom. On the other hand, on the attached Rh dimer, it is not necessary to dissociate any ligands during the catalytic cycle, and hence the Rh dimer acts as an effective catalytic site on SiO_2 . Chemistry of the Rh dimer on the surface is different from chemistry of the homogeneous Rh monomer in a homogeneous system. CO insertion to alkyl on the Rh monomer proceeds only in the presence of excess CO and the acyl decomposes to CO and alkyl under vacuum. In contrast, CO insertion proceeds under vacuum without excess CO and the acyl decomposes in the presence of CO.

The catalytic ethene hydroformylation on Rh_2/SiO_2 is referred to as metal-coordination assisted catalysis by the two adjacent Rh atoms [16,19,32].

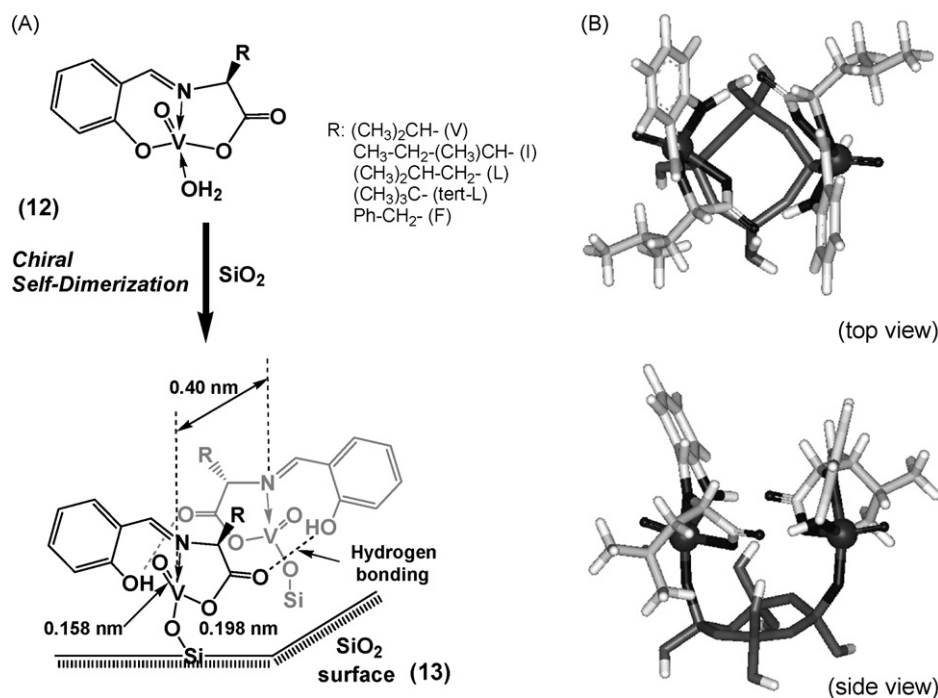
3. Chiral self-dimerized Vanadium Schiff-base complexes on SiO_2 for asymmetric oxidative coupling of 2-naphthol

The fine design of chiral spaces on heterogeneous catalyst surfaces is still a serious challenge to be tackled [4,11,17]. The chemistry of homogeneous metal complexes cannot straightforwardly be transferred to chemistry on heterogeneous surfaces and the enantioselectivity in homogeneous systems often decreases on heterogeneous catalysts by simple immobilization of the homogeneous metal complexes on the surfaces. Thomas et al. proposed immobilization of chiral metal complexes onto mesoporous silica utilizing their special restrictions imposed by the concave surface at which active metal complexes are located [33,34]. Immobilization of chiral metal-complexes on ligand-bonded surfaces has also been achieved for several asymmetric reactions, whose enantioselectivities were similar to those of homogeneous analogues [17,23,24,35,36].

Recently, we found the novel chiral self-dimerization of supported (Vanadium) V-monomer complexes on a SiO_2 surface [20,22], which produces a novel asymmetric reaction space on the surface: two V-monomer complexes with Schiff-base ligands are spontaneously dimerized via a selective reaction with surface Si–OH group and resultant hydrogen bonding. A chiral reaction space is created between two chiral Vanadium centers, which is highly enantioselective for the asymmetric oxidative coupling of 2-naphthol to BINOL with 96% conversion, 100% selectivity to BINOL, and 90% e.e., while the V-monomer precursor is inactive for the oxidative coupling.

Several V-monomer precursors (**12**) with Schiff-base obtained from α -amino acids (L-valine, L-isoleucine, L-leucine, L-tert-leucine, and L-phenylalanine) (Scheme 2(A)) were attached on oxide surfaces by impregnation of each V complex (**12**) in dehydrated ethanol. The V-monomers (**12**) selectively reacted with surface silanols leading to the structural reconstruction of the tridentate Schiff-ligand coordination, as characterized by FT-IR, EPR, XAFS, XPS, XRF, UV–vis, and DFT calculations at each stage during the attachment of the V complex precursor (**12**) and the oxidative coupling of 2-naphthol. The Ph–O moiety of the Schiff-base ligand selectively transformed to Ph–OH configuration via a surface reaction with surface Si–OH, resulting in a coordinatively unsaturated Vanadium conformation on the SiO_2 surface (Scheme 2(A)).

The curve-fitting analysis of Vanadium K-edge EXAFS spectra (Table 2) revealed the local structure of the attached Vanadium complex (**13**) as an unsaturated conformation different from that of the V-monomer precursor (**12**). There are two kinds of chemical bonding of a V=O bond at 0.157 ± 0.001 nm, which is similar to that of the precursor, while the CN of V–O bonds at 0.199 ± 0.002 nm decreased from 3.8 ± 0.4 to 2.8 ± 0.5 after the attachment on the SiO_2 surface (Table 2). The decrease in the CN of V–O by the support was also observed



Scheme 2. Chiral self-dimerization of V Schiff-base complexes on SiO₂ (A) and the top view and side view of a DFT-modeled V-dimer structure (B).

for 0.8, 1.6, and 3.4 wt% V samples independent of V loading. Longer-distance bonding was not observed with all the catalysts, indicating that there was no direct V–V bonding in the supported V catalysts.

EXAFS and FT-IR spectra of the supported V complexes demonstrate the unique surface-attaching reaction accommodated by the surface Si–OH groups. The decrease in the coordination number of V–O(N) bonds indicates that the V cen-

ter becomes unsaturated on the surface. All coordination sites of the Schiff-base ligand to the V⁴⁺ center possess infrared-active functional groups, Ph–O, Ph ring, C=N, and COO as shown in Scheme 2(A): three frequencies (1598, 1373, and 1362 cm^{−1}) are assigned as one $\nu_{\text{asym}}(\text{COO})$ and two $\nu_{\text{sym}}(\text{COO})$; 1629 cm^{−1} peak is assigned to $\nu(\text{C=N})$; four peaks of 1547, 1470, 1447, and 1436 cm^{−1} are referred to $\nu(\text{Ph})$; a strong peak of 1290 cm^{−1} is attributed to $\nu(\text{Ph-O})$ (Table 2). A small difference between

Table 2
Curve-fitting results of EXAFS Fourier transforms ($k = 30\text{--}120\text{ nm}^{-1}$, $R = 0.10\text{--}0.20\text{ nm}$) at V K-edge measured at 16 K and IR vibration frequencies for a Vanadium precursor (L-leucine) (a), its supported Vanadium complex (V: 3.4 wt%) (b), and that treated with 2-naphthol (c)^a

Shell/vibration mode	CN	Distance (Å)	Wavenumber (cm ^{−1})
(a) Precursor			
V=O	1.0	1.58 ± 0.01	
V–O	3.8 ± 0.4	1.98 ± 0.01	
$\nu(\text{C=N})$ ^b			1629
$\nu_{\text{asym}}(\text{COO})$, $\nu_{\text{sym}}(\text{COO})$ ^b			1598, 1373, 1362
$\nu(\text{Ph})$ ^b			1547, 1470, 1447, 1436 ^c
$\nu(\text{Ph-O})$ ^b			1290
(b) Supported V complex			
V=O	1.0	1.57 ± 0.01	
V–O	2.8 ± 0.5	1.99 ± 0.02	
$\nu(\text{C=N})$ ^d			1629
$\nu_{\text{asym}}(\text{COO})$, $\nu_{\text{sym}}(\text{COO})$ ^d			1602, 1370, negligible
$\nu(\text{ph})$ ^d			1554, 1548, 1471, 1452 ^c
$\nu(\text{Ph-O})$ ^d			1391
(c) Treated with 2-naphthol			
V=O	1.0	1.57 ± 0.02	
V–O	4.0 ± 0.6	1.99 ± 0.02	

^a Ref. [22].

^b KBr disk.

^c Relative intensity of the three peaks (1470/1448/1436 cm^{−1}) changed from 1/2.0/1.4 to 1/2.7/0 after the supporting.

^d Neat disk.

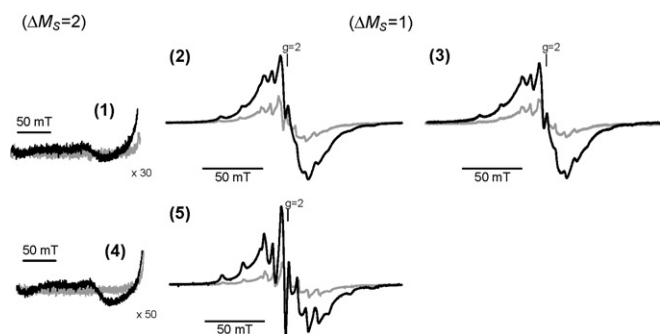


Fig. 2. EPR spectra at 6 K for the SiO₂-supported Vanadium complex (V: 3.4 wt%) (**13**) in the absence (gray line) and presence (black line) of O₂. (1) Half band for the first O₂ adsorption, (2) main signal for the first O₂ adsorption, (3) main signal for the second O₂ adsorption after the evacuation of adsorbed O₂ in the first run, (4) half band after the coordination of 2-naphthol and (5) main signal after the coordination of 2-naphthol.

$\nu_{\text{asym(COO)}}$ and $\nu_{\text{sym(COO)}}$ ($\sim 230 \text{ cm}^{-1}$) indicates the delocalization of electron density on the C=O bond to O–CO, which makes a hydrogen bond with a Ph–OH group of an adjacent V complex discussed hereinafter.

After the attachment on SiO₂, the difference between $\nu_{\text{asym(COO)}}$ and $\nu_{\text{sym(COO)}}$ was also small, which implies that there is hydrogen bonding on C=O, which leads to delocalization of the electron density. The $\nu_{\text{(C=N)}}$, $\nu_{\text{asym(COO)}}$, and $\nu_{\text{sym(COO)}}$ were very similar to those of the precursor, indicating no significant change in the original coordination of these groups upon supporting. On the other hand, the four $\nu_{\text{(Ph)}}$ peaks were different from those of the precursor in both their positions and relative intensities and the $\nu_{\text{(Ph–O)}}$ at 1290 cm^{-1} for the precursor dramatically shifted to 1391 cm^{-1} by the support. Such a large shift was observed on an ionized molecule Ph–O[−], therefore, the large shift of $\nu_{\text{(Ph–O)}}$ and the changes in the intensity ratio of $\nu_{\text{(Ph)}}$ were caused by the structural reconstruction of the Ph–O coordination to produce a new Ph–OH moiety that was promoted by proton transfer from Si–OH. These results demonstrate that the PhO[−] coordination is dispatched from the V center by the reaction of the V precursor with the Si–OH to form Ph–OH group as illustrated in Scheme 2(A) [20,22].

Fig. 2 shows EPR spectra for the SiO₂-supported V complex (**13**) in the presence and absence of O₂ measured at 6 K. The V-monomer precursor (**12**) showed hyperfine signals attributed to d1 configuration of a V=O complex, while a different broad peak was also observed on the hyperfine signals for the supported V complex (**13**) (Fig. 2(2)). It greatly increased after the adsorption of O₂ and the half-band signal was also detected as shown in Fig. 2(1). The results demonstrate that another V complex is located near a V complex to form a dimer assembly.

The V–V distance in the V-dimer produced by self-assembly on the surface is estimated to be $0.40 \pm 0.05 \text{ nm}$ by the relative intensity of the forbidden half-field transition ($|\Delta M_s| = 2$) to the allowed transition ($|\Delta M_s| = 1$) [37]. After evacuation of the O₂-adsorbed sample, the intensity returns completely to the original one and the change in the EPR signal occurs reversibly, which

indicates the reversible adsorption of O₂ molecules on the V-dimer (Fig. 2(3)). Thus the supported V complex (**13**) possesses capacity for O₂ activation that is indispensable for the oxidative coupling reaction. The broad signal and the behavior for oxygen molecules were observed in the range of V loading 0.3–3.4 wt%, indicating that the chiral self-dimerization of the V precursors occurs independent of V loading on the SiO₂ surface.

The Ph–OH moiety formed by the surface reaction of the V-monomer precursor (**12**) with surface OH groups undergoes hydrogen bonding with the C=O group of the ligand in the adjacent V complex to assemble the supported V complexes on the surface (**13**) illustrated in Scheme 2(A). Indeed, a difference (232 cm^{-1}) in the frequencies of $\nu_{\text{asym(COO)}}$ and $\nu_{\text{sym(COO)}}$ in the FT-IR spectrum indicates the occurrence of hydrogen bonding at the C=O oxygen. The V-monomer precursor (**12**) selectively reacted with a surface Si–OH group, followed by the chiral self-dimerization to form a novel V-dimer with hydrogen bonding between Ph–OH and C=O on the surface.

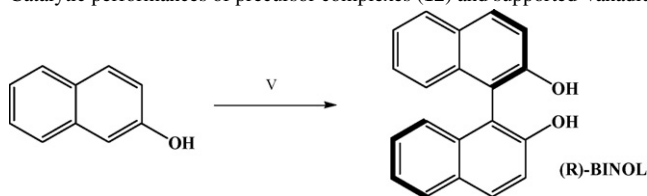
The DFT calculation for the structure of the chiral self-dimerized V-dimer on SiO₂ reveals that two V=O bonds are directed to the opposite sides mutually from the principal molecular plane of the V complex, making chiral V sites, similar to a structural unit in the V complex crystal [38]. The DFT modeling also depicts that a favorable reaction space for the oxidative coupling of two 2-naphthols in the chiral pocket is created between the two unsaturated chiral V centers (Scheme 2(B)).

The supported V-dimer catalysts (**13**) were active for the coupling of 2-naphthol under aerobic conditions, while the homogeneous V precursor (**12**) is inactive for the reaction (Table 3). On the SiO₂-supported V catalysts (**13**), the conversion reaches maximum 96%, and the reaction rate in toluene is 1.3 times higher than that in CHCl₃. The supported V catalyst (**13**) is perfectly selective (100% selectivity) and reusable for the BINOL synthesis. On the other hand, Al₂O₃ and TiO₂ were not suitable as supports for the V precursor (**12**), leading to low selectivities for BINOL.

Enantioselectivity was not modified by the chiral alkyl groups of Schiff-base ligands: there are no significant differences in the performances between the catalysts derived from L-isoleucine (51% e.e.), L-leucine (54% e.e.), and L-phenylalanine (56% e.e.) in CHCl₃. The most bulky ligand L-tert-leucine has a tert-butyl group neighboring to the V reaction site, but it reduced the enantioselectivity. These two alkyl groups overhang outside the V complexes (**13**) illustrated in Scheme 2(A), and seemingly they did not affect the asymmetric coupling of 2-naphthol.

The Vanadium loading on SiO₂ including an L-leucine segment was varied in the V loading range 0.3–3.4 wt% in order to maximize enantioselectivity for the coupling reaction (Table 3). No leaching of V complexes was observed for all the supported catalysts in toluene. Accompanied with an increase in V loading 0.3, 0.8, 1.6, and 3.4 wt%, the enantioselectivity dramatically increased: 32% e.e., 39% e.e., 48% e.e., and 90% e.e., respectively, as shown in Table 3. The 3.4 wt% Vanadium catalyst corresponding to full coverage of the V complex exhibited 90% e.e., which is comparable to the best performance for the coupling of 2-naphthol on a homogeneous catalyst reported thus far [39–42]. Furthermore, the supported V catalysts can be reused

Table 3

Catalytic performances of precursor complexes (**12**) and supported Vanadium dimer (**13**) for asymmetric 2-naphthol coupling^a

Catalyst–ligand ^b	Temperature (°C)	Time (day)	Solvent	Conversion (%)	Selectivity (%)	% e.e. (R)
Precursor–L ^c	20	5	CHCl ₃	0	0	–
V–L/SiO ₂ 0.3 wt%	–10	5	CHCl ₃	9	100	54
V–L/SiO ₂ 0.3 wt%	20	5	Toluene	96	100	13
V–L/Al ₂ O ₃ 1.7 wt%	20	5	CHCl ₃	69	53	–2
V–L/TiO ₂ 0.8 wt%	20	5	CHCl ₃	52	0	–
V–V/SiO ₂ 0.3 wt%	20	5	Toluene	99	100	5
V–V/SiO ₂ 0.3 wt%	–10	6	Toluene	12	100	14
V– <i>tert</i> -L/SiO ₂ 0.3 wt%	–10	5	Toluene	11	100	12
V–L/SiO ₂ 0.3 wt%	–10	5	Toluene	11	100	32
V–L/SiO ₂ 0.3 wt% ^d	–10	5	Toluene	10	100	33
V–L/SiO ₂ 0.8 wt%	–10	5	Toluene	33	100	39
V–L/SiO ₂ 1.6 wt%	–10	5	Toluene	42	100	48
V–L/SiO ₂ 3.4 wt%	–10	5	Toluene	93	100	90
V–L/SiO ₂ 3.4 wt% ^d	–10	5	Toluene	91	100	89

^a Ref. [22]. Catalyst 100 mg, toluene 5 ml, the molar ratio of Vanadium dimer/2-naphthol was 1/36.^b L: L-leucine, V: L-valine, *tert*-L: L-*tert*-leucine.^c Homogeneous reaction.^d Reused.

after filtration and exhibited similar catalytic performances as shown in Table 3. From the estimation of the cross section of the V precursor, the V loading of 3.4 wt% corresponds to full coverage of the complex on the SiO₂ surface, where the configuration and reaction environment of the V-dimer on the surface are regulated rigidly for the achievement of higher enantioselectivity when compared to the lower V loadings.

The reactant 2-naphthol coordinates to the unsaturated V center, whose V–O bond coordination number increased from 2.8 to 4.0 as shown in Table 2. The unsaturated V site can activate one 2-naphthol molecule: thus the V-dimer unit is favorable for the coupling of two molecules. After the coordination of 2-naphthol, the V-dimer also coordinates O₂ between two adjacent V sites, whose EPR spectra are presented in Fig. 2(4) and (5). No positive formation of BINOL under an N₂ atmosphere demonstrated that the 2-naphthol coupling proceeds on the O₂-activated V-dimer on SiO₂ [22].

The enantioselectivity of the coupling reaction is determined by the chiral conformation on the V center rather than the chirality of Schiff-base ligands. The chirality of the ligands sterically affects the chiral self-dimerization of V complexes on the surface, and the chiral ligands themselves do not determine the enantioselectivity for the 2-naphthol coupling. The increase in V loading on SiO₂ achieved the higher regulation of mobility of the assembled V species on the surfaces, resulting in the high enantioselectivity (90% e.e.) at 93% conversion on the V 3.4 wt% catalyst compared to the case of the V 0.3 wt% catalyst with the same V structure (Table 3). The selective transformation of metal coordination at the SiO₂ surface produces a unique reaction space for the selective oxidation.

4. N-interstitial Re₁₀-cluster catalyst on HZSM-5 zeolite for the direct phenol synthesis from benzene and O₂

Re is known to be one of oxophilic atoms with various valences [43,44]. Various oxide compounds of V, Mn, Mo, and W are widely used for selective oxidation using O₂, while exploitation of Re catalysts for selective oxidation are still undeveloped because of sublimation of Re oxides like Re₂O₇ under oxidation reaction conditions. Several arrangements of ReOx species with chemical interaction with various oxide supports and their unique catalytic properties were observed, different from those on single Re oxides [45–48]. For example, ReOx supported on Fe₂O₃ behaves as a highly selective catalyst for one-step methylal synthesis from three molecules of methanol and molecular oxygen [49,50]; the octahedral ReOx cluster in zeolite pores was active for propene oxidation/ammoxidation with NH₃ [51,52], indicating that Re species work as well as oxidation catalysts under a reductive atmosphere.

The HZSM-5 zeolite-supported novel N-interstitial Re₁₀ cluster was active for the direct phenol synthesis from benzene and O₂ in the presence of NH₃ [30]. Phenol, which is produced by three-step cumene process, is one of the major products in industry. However economically and environmentally favorable benzene–O₂ catalytic systems with high selectivity for phenol synthesis have not been discovered to date because molecular oxygen is difficult to activate selectively to oxidize benzene to phenol. The acidity and pore structure of HZSM-5 lead to a novel N-interstitial Re₁₀ cluster, which cannot be produced on other oxide surfaces or in solutions, and the direct phenol synthesis using O₂ as a sole oxidant was achieved with the highest phenol

Table 4a

Catalytic performances of Re/zeolite catalysts for the direct phenol synthesis at 553 K under steady-state reaction conditions^a

Catalyst	SiO ₂ /Al ₂ O ₃	Method	Re (wt%)	TOF ($\times 10^{-5} \text{ s}^{-1}$) ^b	PhOH selectivity (%)
HZSM-5	19	–	–	Trace	0
Re/HZSM-5 ^c	19	CVD	0.58	Trace	0
Re/HZSM-5	19	CVD	0.58	65.6	87.7
Re/HZSM-5 ^d	19	CVD	2.2	83.8	82.4
Re/HZSM-5	19	Imp.	0.6	11.8	27.7
Re/HZSM-5	24	CVD	0.58	36.2	68.0
Re/HZSM-5	39	CVD	0.59	31.0	48.0
Re/H-Beta	37	CVD	0.53	18.5	12.0
Re/H-USY	29	CVD	0.60	Trace	0
Re/H-Mordenite	220	CVD	0.55	26.3	23.4

^a Ref. [30]. Catalyst 0.20 g; W/F = 6.7 g_{cat} h mol⁻¹; He/O₂/NH₃/benzene = 46.4/12.0/35.0/6.6 (mol%).^b Consumed benzene/Re/s.^c In the absence of NH₃.^d W/F = 10.9 g_{cat} h mol⁻¹; He/O₂/NH₃/benzene = 46.4/12.0/35.0/6.6 (mol%).

yield (10% conversion and 94% selectivity) for the first time [30,31].

Zeolite-supported Re catalysts were synthesized by chemical vapor deposition (CVD) of MTO (CH₃ReO₃) (**14**) with several zeolites such as HZSM-5, H-Beta, H-USY, and H-Mordenite. HZSM-5, which was the best zeolite support for the phenol synthesis, was prepared through changing its Al proportion. For comparison, conventional impregnated catalysts were prepared with water solution of NH₄ReO₄. All catalysts were pretreated at 673 K in a He flow before use.

Table 4a shows the catalytic performances of the Re/zeolite catalysts under steady-state conditions for the selective oxidation of benzene with O₂. A Re-CVD/HZSM-5 catalyst (SiO₂/Al₂O₃ = 19) preferentially produced phenol with 87.7% selectivity in the presence of NH₃ (Table 4a). No other liquid products were detected and the only by-product was gaseous CO₂. The phenol selectivity highly depends on the structures, acid strengths, and SiO₂/Al₂O₃ ratios of zeolites as shown in Table 4a: the rate of phenol formation decreased in the order; HZSM-5 (SiO₂/Al₂O₃ = 19) > HZSM-5 (SiO₂/Al₂O₃ = 24) > HZSM-5 (SiO₂/Al₂O₃ = 39) >> H-Mordenite > H-beta > H-USY. Thus HZSM-5 (SiO₂/Al₂O₃ = 19) among the zeolites employed is the most favorable support for the Re species. The results also suggest that Al–OH in the HZSM-5 framework is a coordination site for active Re species.

Impregnation and physical-mixed Re catalysts were much less active and much less selective for phenol synthesis (Table 4a). The CVD catalyst was almost 18 times more active than the conventional impregnation catalyst. In the physical mixed and impregnated catalysts, the Re⁷⁺ precursors were transformed to partly aggregate as ReO₂ in the presence of the NH₃ reductant and such ill-defined Re aggregates widely decreased both activity and phenol selectivity as shown in Table 4a.

The coexistence of NH₃ is indispensable for selective benzene oxidation. Neither benzene oxidation nor combustion proceeded in the absence of NH₃ (Table 4a). The addition of H₂O and N₂O gave no positive effects on the catalytic performance. Other amine compounds also did not produce any phenol

molecules. The phenol formation rate and selectivity increased with increasing NH₃ pressure because the coexisting NH₃ produces active Re clusters as described hereinafter, and reached maxima around 35–42 kPa of partial NH₃ pressure.

Reaction with NH₃ at 553 K dramatically changed the structure of the supported Re species: Re L_{III}-edge EXAFS showed direct Re–Re interaction at 0.276 ± 0.002 nm, whose coordination number (CN) was 5.2 ± 0.3 (Fig. 3(1)). Two other types of coordination were observed: Re–N/O at 0.204 ± 0.001 nm (CN = 2.8 ± 0.3) and Re=O bonds at 0.172 ± 0.001 nm (CN = 0.3 ± 0.2). The major contribution of metal–metal interaction was through the formation of Re clusters in HZSM-5. Assuming that Re-oxide materials tend to have Re₆ octahedral structures [52,53], the CN of Re–Re bonds of 5.2 indicates Re₁₀ clusters edge-shared with two Re₆ octahedra, whose structure was revealed by DFT calculation (Scheme 3). Interestingly, the Re clusters contained the stoichiometric amount of N₂ (N₂ per Re₁₀) releasing it at 685 K. The interstitial nitrogen atoms are the key element to stabilize the Re₁₀ clusters. Neither the hollow-site nitrogen (Re₃–N), bridged nitrogen (Re–N–Re), nor bridge NH species (Re–NH–Re) stabilized the cluster framework with Re–Re bonds at 0.276 ± 0.002 nm determined by EXAFS [30].

Pulse reactions on the N-interstitial Re₁₀ cluster revealed that the lattice oxygen of the Re₁₀ cluster was inactive for the phenol synthesis. There was no phenol formation from benzene in the absence of O₂ as shown in Table 4b. On the other hand, the N-interstitial Re₁₀ cluster produced by NH₃ selectively converted benzene to phenol in the presence of O₂. The phenol selectivity was 94%, which is the highest phenol selectivity on the direct phenol synthesis using O₂. The selective benzene oxidation with molecular oxygen on the active Re₁₀ clusters proceeds without NH₃, demonstrating that the N-interstitial Re₁₀ cluster is the active species for the direct phenol synthesis. NH₃ has a role to produce the active structure and is not related to the phenol synthesis. After the reactions with benzene and O₂, the catalytically active Re₁₀ cluster was converted to inactive Re monomers as shown in Scheme 3(A).

NH₃ promotes the clusterization of the Re species as a reductant, supplying N atoms to stabilize the Re₆ cluster framework.

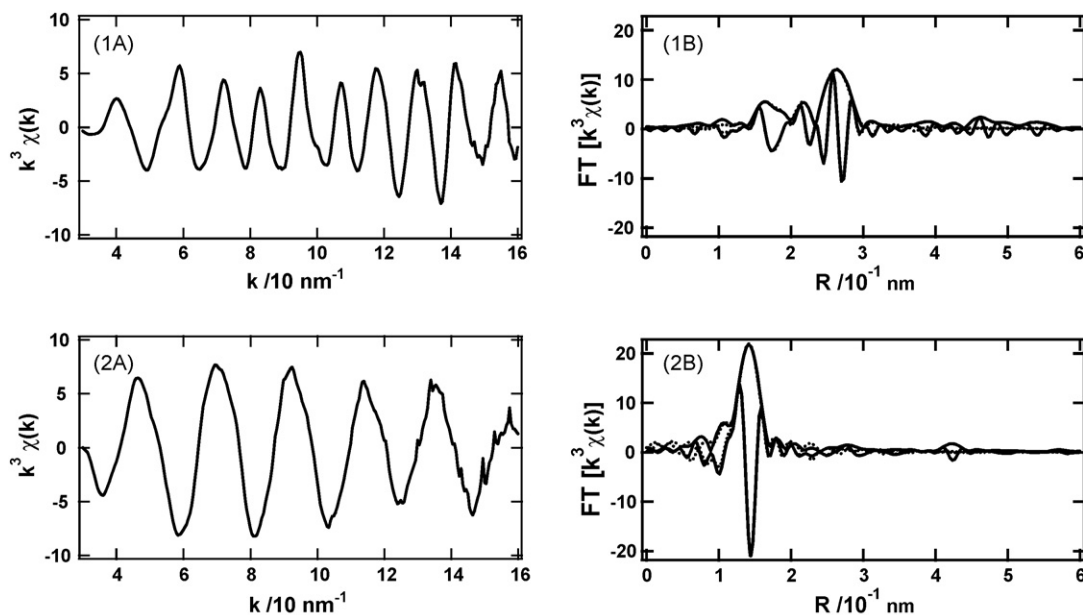
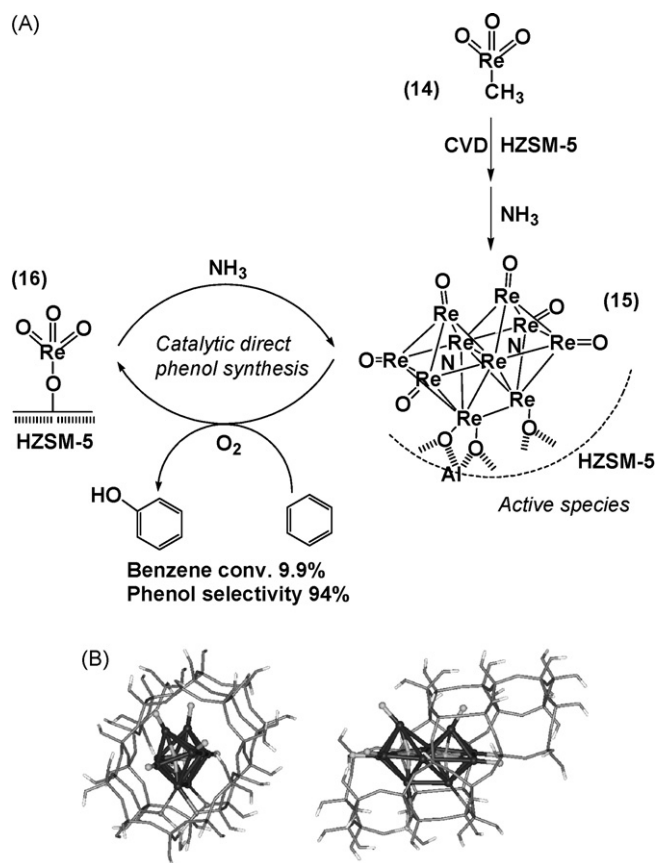


Fig. 3. Rhenium L_{III} -edge EXAFS oscillations (A) and their Fourier transforms (B) of HZSM-5 supported Re catalysts. (1) After the treatment with NH_3 at 553 K for 2 h (**15**) and (2) after the reaction with benzene and O_2 at 553 K (**16**). Solid and dotted lines in (B) represent observed and fitted spectra (both absolute and imaginary parts), respectively.



Scheme 3. (A) Preparation of the HZSM-5 supported Re catalysts by CH_3ReO_3 . NH_3 produces the N-interstitial Re_{10} cluster (**15**), which is the active species for the direct phenol synthesis. (B) Its DFT-modeled structure of the N-interstitial Re_{10} cluster (**15**) supported in three-dimensional pore of HZSM-5 (pore view and side view).

The pore size of HZSM-5 is 5.5 Å, which is similar to the size of the Re_6 -octahedral cluster framework. The HZSM-5 pore structure is supposed to prohibit the further clusterization of the Re catalyst and also the subsequent reaction of the desired phenol. The synergy of coordination of the N-interstitial Re cluster and the three-dimensional pore of HZSM-5 makes possible the highly selective phenol synthesis from benzene and O_2 .

5. Molecular-imprinted metal-complex catalysts on oxide surfaces for tailor-made shape-selective catalysis

5.1. General strategy of molecular-imprinted supported metal complexes

To prepare artificial enzymatic systems possessing the ability to recognize particular substrate molecules, molecular imprinting methods [54–62] which create template-shape cavities with memory of the template molecules in polymer matrices have

Table 4b

Catalytic performance of the CVD-Re/HZSM-5 ($SiO_2/Al_2O_3 = 19$) catalyst (Re: 0.58 wt%) for direct phenol synthesis in the pulse reactions at 553 K in the absence of NH_3 ^a

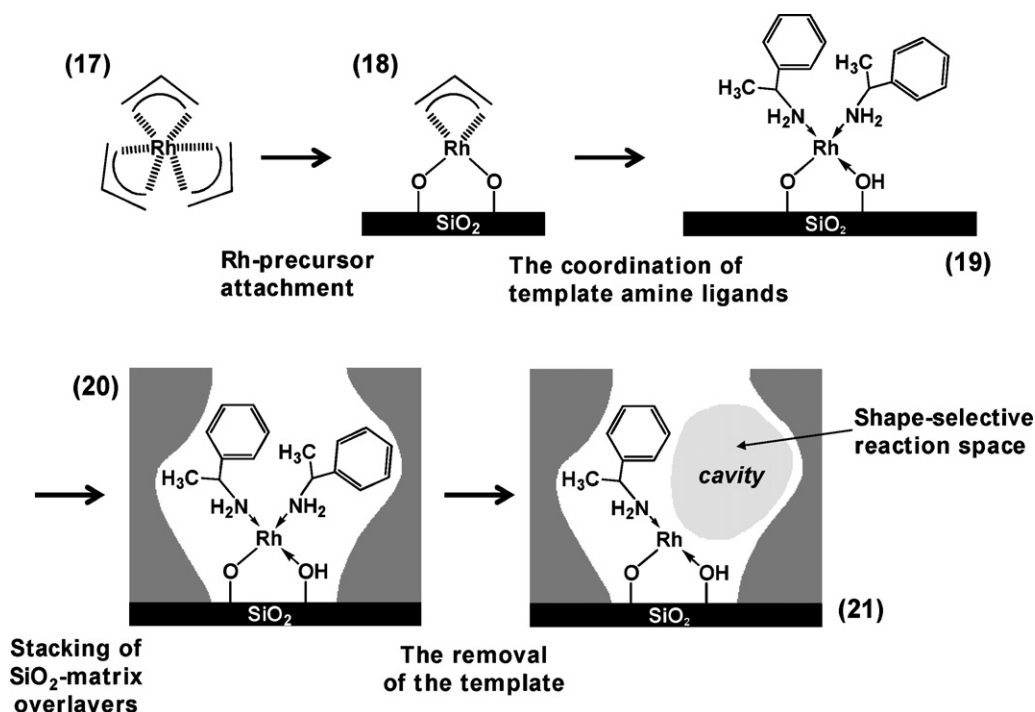
NH_3 treatment at 553 K (h)	Reactant	TOF ($\times 10^{-5} s^{-1}$)	PhOH selectivity (%)
2	Benzene ^b	0	0
2	Benzene + O_2 ^c	74.6	93.9
2 ^d	Benzene + O_2 ^c	86.1	90.6
0	Benzene ^b	0	0
0	Benzene + O_2 ^c	0	0

^a Ref. [30]. Catalyst 0.10 g.

^b 1 pulse of benzene (He/benzene = 93.4/6.6 (mol%)).

^c 1 pulse of benzene + O_2 (He/ O_2 /benzene = 81.4/12.0/6.6 (mol%)).

^d Catalyst: 1.0 g.

Scheme 4. Preparation of a molecular-imprinted Rh-amine monomer catalyst on a SiO_2 surface.

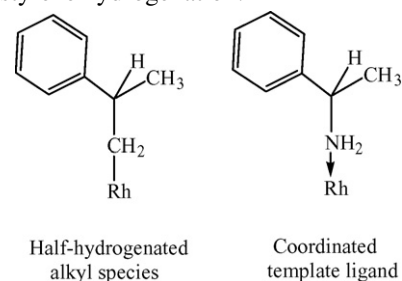
been developed. They have been established in receptor, chromatographic separations, fine chemical sensing, etc. in the past decade, and are regulated mainly by simple adsorption on the imprinted sites. Nevertheless, artificial enzymatic materials synthesized by molecular imprinting techniques using a variety of template molecules provide promising molecular recognition catalysis with 100% selectivity for a variety of catalytic reactions where natural enzymes cannot be employed.

Recently, in addition to imprinted acid–base catalysts [63–67], attempts to imprint metal complexes have been reported and constitute current state of the art [25–29,68–79]. In most metal-complex imprinting, ligands are used as template molecules to create a cavity near the metal site. Molecular imprinting of metal complexes enables one to realize several features; (1) attachment of metal complex on robust supports, (2) surrounding of the metal complex by polymer matrix, and (3) production of shape selective cavity at the metal site. Metal complexes thus imprinted have been applied to molecular recognition [68,69], reactive complex stabilization [70], ligand exchange reaction [71], and catalysis [25–72]. Most of the imprinted metal-complex catalysts have been prepared by imprinting in bulk polymer, and we have proposed molecular imprinting of supported metal complexes on oxide surfaces for the first time [25–29]. The strategy to design active and selective catalysts was based on the following five factors for regulation, (1) conformation of ligands coordinated to Rh atom, (2) orientation of vacant site on Rh, (3) cavity with the template molecular shape for reaction space produced following template removal, (4) architecture of the cavity wall, and (5) micropores in the inorganic polymer-matrix overlayers stabilizing the active species at the surface.

5.2. An amine-imprinted Rh monomer catalyst on SiO_2 and its enzymatic inhibition of alkene hydrogenation

There are many stable amine ligands with various shapes commercially available. Thus, we chose an amine ligand as a template molecule for the preparation of a molecular-imprinted Rh complex catalyst on SiO_2 . Scheme 4 illustrates the schematic procedure of amine-imprinted Rh monomer catalyst on a SiO_2 surface [29].

$\text{Rh}(\eta^3\text{-C}_3\text{H}_5)_3$ (17) was used as a monomeric precursor and is easily attached on SiO_2 releasing C_3H_6 as shown in Scheme 4. On SiO_2 , two propene molecules are evolved through the stoichiometric reaction of (17) with two surface silanol groups (Scheme 4). The next step is the coordination of an amine template to the attached Rh complex $[\text{Rh}(\eta^3\text{-C}_3\text{H}_5)(\text{OSi})_2]$ (18). α -Methylbenzylamine was chosen as a template ligand because it has a similar shape to a half-hydrogenated intermediate species in α -methylstyrene hydrogenation:



Thus, the space following the removal of the template will be a shape selective reaction space. As many amine compounds are available, many kinds of shape selective sites can be prepared in the similar way.

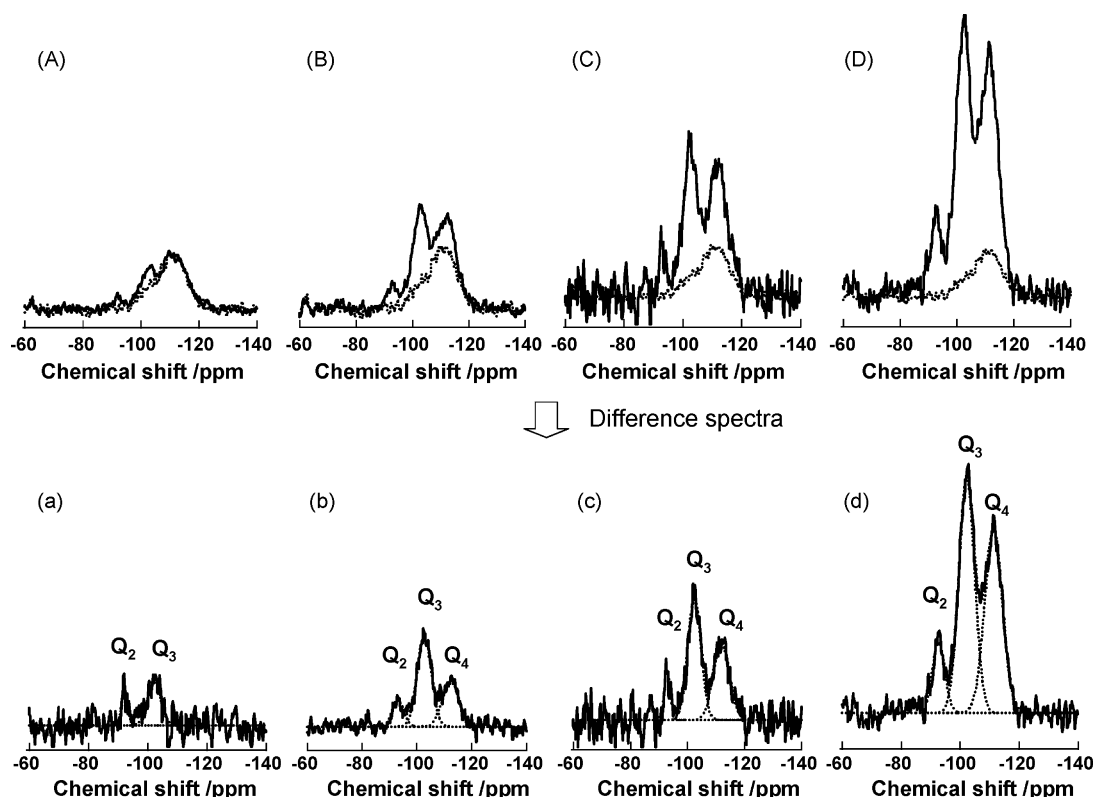


Fig. 4. ^{29}Si solid-state NMR spectra for imprinted materials prepared by the chemical vapor deposition and hydrolysis-polymerization of $\text{Si}(\text{OCH}_3)_4$. (A)–(D) solid lines represent the imprinted materials on SiO_2 , and dotted lines correspond to the SiO_2 support. (a)–(d) Their difference spectra, which correspond to be SiO_2 -matrix overlayers. (a) 1.4 monolayer (ML), (b): 4.7 ML, (c): 9.3 ML, and (d): 15.9 ML.

The third step of surface molecular imprinting is the stacking of SiO_2 -matrix overlayers on the SiO_2 surface using $\text{Si}(\text{OCH}_3)_4$ as a polymerizing reagent. $\text{Si}(\text{OCH}_3)_4$ earned some excellent printing results: (1) the stacking of SiO_2 network proceeds layer by layer to form SiO_2 -matrix overlayers on a SiO_2 support; (2) $\text{Si}(\text{OCH}_3)_4$ reacts with surface silanol groups preferentially, and the polymerization does not occur in the absence of surface silanols under the present conditions; (3) as a result, the height of the matrix overlayers from the surface is controlled, pores including attached Rh complexes are produced in the SiO_2 -matrix overlayers, and the attached Rh complexes are not buried in the surface-matrix overlayers; (4) the SiO_2 matrix possesses a lot of silanol groups (Q_3 and Q_2) to be flexible enough to shape the template figure.

The structures of SiO_2 -matrix overlayers prepared by hydrolysis-polymerization of $\text{Si}(\text{OCH}_3)_4$ were confirmed by ^{29}Si solid-state MAS NMR as shown in Fig. 4. When $\text{Si}(\text{OCH}_3)_4$ corresponding to be a monolayer of the SiO_2 surface was used, only surface species (Q_2 and Q_3) were observed (Fig. 4(a)). This means that the hydrolysis-polymerization occurs with surface-OH groups at the SiO_2 surface. When the amount of $\text{Si}(\text{OCH}_3)_4$ increased, bulk Q_4 species appeared as shown in Fig. 4(b)–(d). The large proportions of surface Q_2 and Q_3 species indicate that the network of the surface SiO_2 -matrix overlayers seems to have a flexible structure with many Si–OH groups, which is quite essential for good imprinting [28].

After the stacking of the SiO_2 -matrix overlayers, the local coordination of the supported Rh complex (**20**) did not change

and following evacuation at 373 K promoted the elimination of the amine ligand. The coordination number (CN) of the Rh–N interaction declined from 4 (**20**) to 3 (**21**) approximately, and the Rh–N distance shortened from 0.209 (± 0.001) nm to 0.205 (± 0.001) nm. The decrease in CN suggests the elimination of one ligand as shown in Scheme 4. The H_2 adsorption experiments reveal that the surface pores over the Rh complexes are preserved in the stacking of SiO_2 -matrix overlayers. The number of adsorbed H_2 per Rh is about 1 as described above, indicating that almost all the Rh complexes can act as active sites for hydrogenation catalysis [29].

$\text{Rh}(\text{C}_3\text{H}_5)_3$ (**17**), $\text{Rh}(\text{C}_3\text{H}_5)/\text{SiO}_2$ (**18**), supported Rh complex with two amines (**19**), and imprinted Rh catalyst with one amine (**21**) were used as catalysts for the hydrogenation of α -methylstyrene. The homogeneous complex (**17**) has no catalytic activity for the hydrogenation and decomposes rapidly under the reaction conditions. The reaction also did not proceed after the decomposition. On the other hand, the attached Rh complex, (**18**) also brought about decomposition to form Rh aggregates under the reaction conditions. The initial activity of (**18**) is zero, but the ill-defined decomposed species exhibits some catalytic activity. Similar behavior is also observed on (**19**) as shown in Fig. 5(B), where the decomposition of the attached complex occurs with color change and the catalytic activity is eventually lost. Such metal aggregates lose the property and shape selectivity of intrinsic metal complexes.

On the other hand, (**21**), after the removal of the template amine, has a high hydrogenation activity ($\text{TOF} = 5.2 \text{ min}^{-1}$)

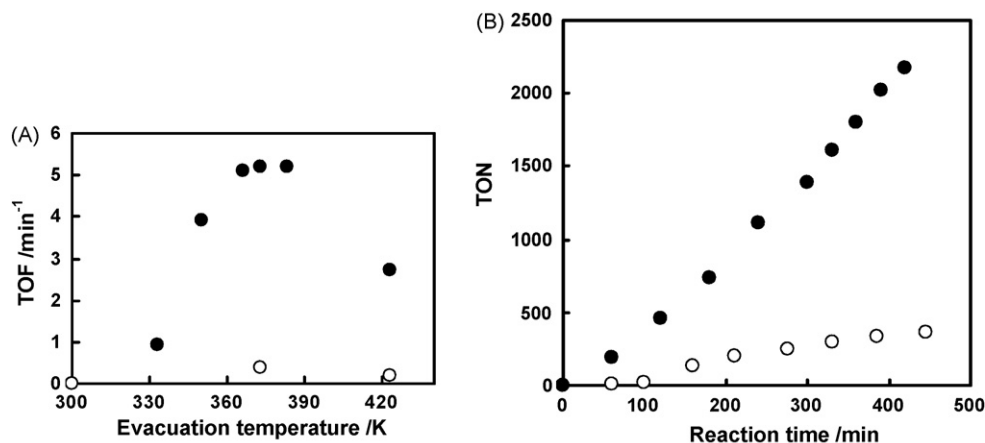


Fig. 5. (A) Reaction rates (TOFs: turnover frequencies) for α -methylstyrene hydrogenation of the supported Rh-amine catalyst (**19**) (○) and the imprinted Rh-amine catalyst (**20**) (●) against evacuation temperature for the removal of the template amine ligand. The supported catalyst (**19**) without SiO₂-matrix overlayers loses its catalytic activity by heating, while the imprinted catalyst (**20**) with SiO₂-matrix overlayers exhibits high catalytic activity after the removal of the template. (B) Turnover numbers for α -methylstyrene hydrogenation of the supported Rh-amine catalyst (**19**) (○) and the imprinted Rh-amine catalyst with the unsaturated Rh center after the removal of the template (**21**) (●).

under identical conditions (Fig. 5). Furthermore, the reaction proceeds linearly, and the Rh structure is maintained after the reaction; (**21**) is durable and reusable as shown in Fig. 5(B). The stability and durability of the coordinatively unsaturated Rh species (**21**) are derived from the location of the complex and the wall architecture of the SiO₂-matrix overlayers, which inhibit the Rh species from decomposing.

The catalytic activity depends highly on the evacuation temperature for the elimination of the template as shown in Fig. 5(A). The catalytic activity increases with increase in the evacuation temperature. The maximum activity is accomplished in the temperature range 363–383 K, and at higher temperature the activity decreases due to dissociation of the amine as shown in Fig. 5(A). The increase in the catalytic activity is parallel to the structural change (decrease in the CN of Rh–N) derived from the EXAFS analysis. Thus, only the imprinted Rh catalyst with the unsaturated Rh center is the active species for the catalytic hydrogenation reaction after the removal of the template amine.

As amines easily coordinate to an unsaturated Rh complex and (**19**) with two amine ligands has no hydrogenation activity, amines are regarded as effective reaction inhibitors for the unsaturated Rh complex (**21**). The smaller benzylamine (Inh. a) behaves as a similar inhibitor to the template (Inh. b), which indicates that the template cavity does not affect smaller molecules than the template (Fig. 6). In contrast, significant differences among the larger amine inhibitors were observed. One methyl substitution on the phenyl ring (Inh. c) makes it hard to coordinate to Rh, exhibiting less inhibition (Inh. c). The order of inhibition to the α -methylstyrene hydrogenation was Inh. a \approx Inh. b (template) < Inh. c < Inh. d < Inh. e \approx Inh. f < Inh. g as shown in Fig. 6. A phenyl ring of the naphthyl group (Inh. g) is more effective for inhibition than the other phenyl branch of Inh. f as shown in Fig. 6. These results suggest that the shape and size of the phenyl plane of the inhibitors are much more effective compared to those on the other sp³ carbon atom [29].

Coordinatively unsaturated metal sites are crucial for effective catalysis. The strategy of surface molecular imprinting

makes three essentials possible: (1) the formation of unsaturated active metal sites, (2) shape-selective reaction space on the active metal center, and (3) high durability of the unsaturated metal center by surface matrix overlayers. Fine shape selectivity for simple molecules without any functional groups which is one of the most difficult regulations in catalysis can be designed at the surface and this method can be applied for other template molecules, metal complexes, and catalytic reactions.

5.3. A molecular-imprinted Rh dimer catalyst on SiO₂ for highly shape-selective hydrogenation

A molecular-imprinted Rh dimer can be prepared in a similar manner using Rh₂Cl₂(CO)₄ (**22**) precursor and P(OCH₃)₃, which is regarded as an analogue to a half-hydrogenated alkyl intermediate of hydrogenation of 3-ethyl-2-pentene [26–28]. Rh₂Cl₂(CO)₄ (**22**) was attached on SiO₂ retaining its dimer structure. By exposing to P(OCH₃)₃, the surface-attached Rh

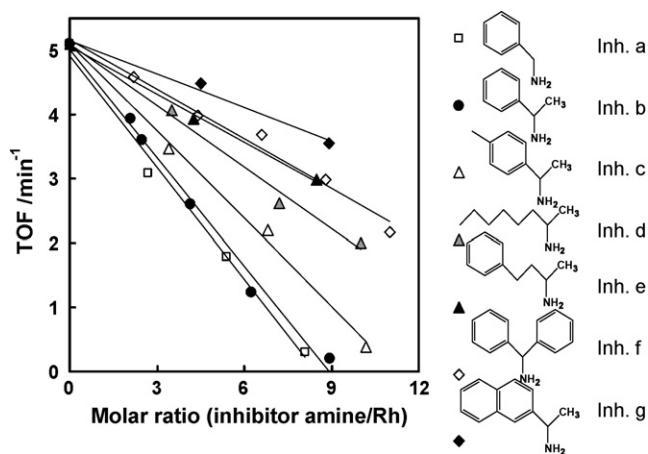


Fig. 6. Shape-selective inhibition of α -methylstyrene hydrogenation on the molecular-imprinted Rh-amine catalyst (**21**) with seven amine inhibitors with different shapes (Inh. a–Inh. g).

carbonyl dimer (**23**) was converted to a Rh monomer pair (**24**) with two $\text{P}(\text{OCH}_3)_3$ ligands on Rh accompanied by Rh–Rh bond breaking (Rh–P: 0.224 nm; no Rh–Rh bond by EXAFS), which was attached on the surface via Rh–O bonding at 0.203 nm in a bidentate form (Scheme 4). After the $\text{P}(\text{OCH}_3)_3$ coordination the first step of molecular imprinting for the attached rhodium complexes is a hydrolysis-polymerization of $\text{Si}(\text{OCH}_3)_4$, which possesses methoxy groups with positive interaction with the template.

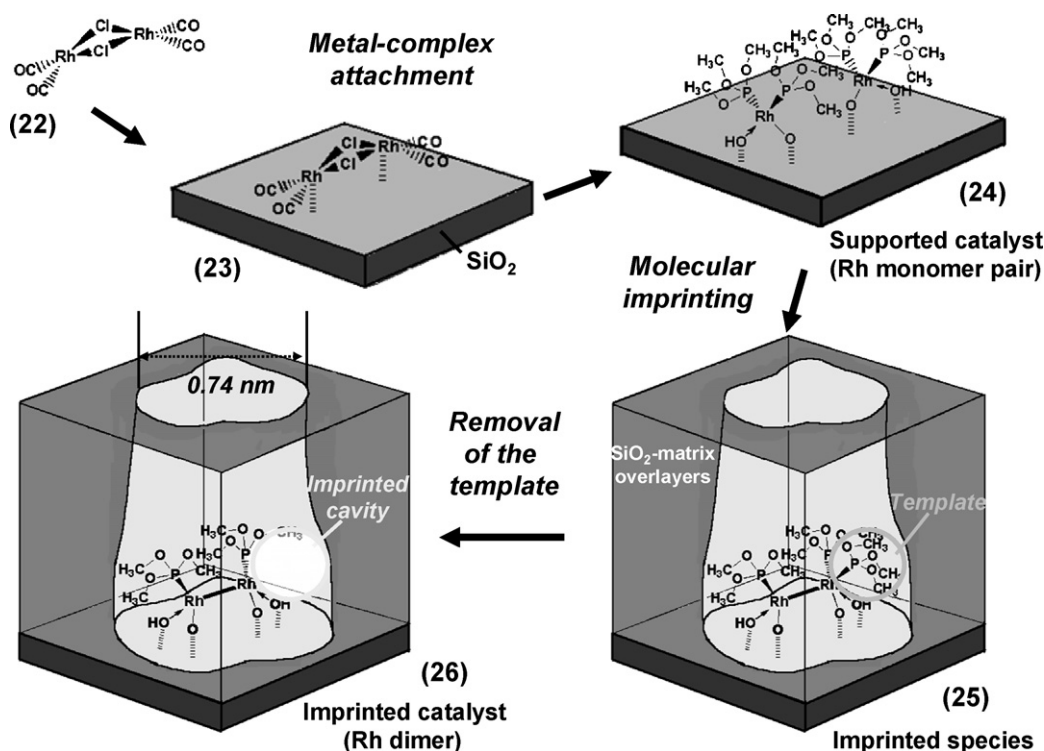
The second step is the removal of the template by evacuation at 363 K to produce the imprinted Rh dimer catalyst (**26**). Note that the surface imprinting causes dimerization of the Rh monomers (**24**) to produce highly active Rh dimers (**26**) with a direct Rh–Rh bond at 0.268 nm in the pores of 0.74 nm dimension in the SiO_2 -matrix overlayers on the SiO_2 surface. The EXAFS analysis also indicated the removal of a phosphite ligand and per Rh by the molecular imprinting procedure, where the coordination number of Rh–P bond (0.221 nm) calculated by the EXAFS analysis decreases from 2.3 to 1.1. A large decrease in Rh 3d XPS intensity after the stacking of SiO_2 -matrix overlayers demonstrated that the Rh species were embedded in the polymerized silica matrix overlayers that were characterized by ^{29}Si solid-state MAS NMR. The height of the matrix overlayers was estimated to be 1.9 nm (Scheme 5).

DFT calculations for the imprinting process revealed the structure of an imprinted species. When $[\text{Rh}(\text{P}(\text{OCH}_3)_3)_2]_2$ (**24**) with a Rh–Rh distance of 0.306 nm (no direct bonding) eliminated a $\text{P}(\text{OCH}_3)_3$ ligand, leading to a reduction in steric hindrance, a direct Rh–Rh bond at 0.271 nm was formed to stabilize the unsaturated structure as $\text{Rh}_2(\text{P}(\text{OCH}_3)_3)_3$ (**25**). When the SiO_2 -matrix overlayers were stacked surrounding the sup-

ported Rh monomer pair, the intermediate (**25**) was proposed as an imprinted species. The final evacuation at 373 K promoted the further elimination of one more $\text{P}(\text{OCH}_3)_3$ ligand and an imprinted cavity with the shape of a $\text{P}(\text{OCH}_3)_3$ ligand was created at the surface.

Table 5 shows steady-state reaction rates (turnover frequencies (TOFs)) of the hydrogenation of eight alkenes at 348 K on the supported Rh monomer pair (**24**) and the imprinted Rh dimer (**26**). The homogeneous complexes $\text{Rh}_2\text{Cl}_2(\text{CO})_4$ (**22**) and $\text{RhCl}(\text{P}(\text{OCH}_3)_3)_3$ and the supported species $\text{Rh}_2\text{Cl}_2(\text{CO})_4/\text{SiO}_2$ (**23**) show no activities for the reaction. On the other hand, the species (**24**) exhibits significant catalytic activity under similar reaction conditions. The hydrogenation reactions are remarkably promoted by the surface imprinting. The species (**26**) is extremely active for alkene hydrogenation. For example, the hydrogenation of 2-pentene is very significantly promoted (51 times greater TOF) when compared to that on species (**24**). The metal–metal bonding and coordinative unsaturation of the Rh dimer are key factors for the remarkable activity of the species (**26**). The species (**26**) is highly durable and surprisingly air-stable in spite of its unsaturated structure, which is advantageous in the practical handling of the system. Further, it can be reused without any loss of catalytic activity [27].

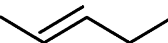
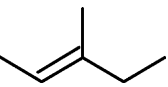
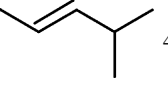
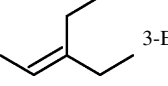
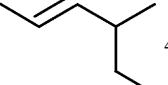
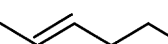
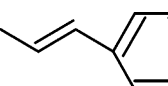
The ratios of TOFs corresponding to the degree of enhancement of the reaction rates, by the imprinting, revealed that species (**26**) showed size- and shape-selectivities for the alkenes as shown in Table 5. Selectivity for the alkene hydrogenation on species (**26**) depended on the size and shape of the template cavity as a reaction site in the micropores of the SiO_2 -matrix overlayers on the SiO_2 surface in addition to the electronic



Scheme 5. Preparation of a molecular-imprinted Rh dimer catalyst on a SiO_2 surface.

Table 5

Degree of enhancement of the reaction rates on Rh dimer catalysts by molecular imprinting (ratio of TOFs), activation energies (E_a), and activation entropies ($\Delta^\ddagger S$) for the catalytic hydrogenation of alkenes at 348 K^a

Reactant	(24) TOF (s ⁻¹)	(26) TOF (s ⁻¹)	Ratio of TOFs ^b	(24)		(26)	
				E_a^c	$\Delta^\ddagger S^d$	E_a^c	$\Delta^\ddagger S^d$
 2-Pentene	1.3×10^{-3}	6.6×10^{-2}	51	34	−205	26	−195
 3-Methyl-2-pentene	7.0×10^{-5}	3.6×10^{-3}	51	44	−200	43	−170
 4-Methyl-2-pentene	1.3×10^{-4}	5.9×10^{-3}	45	40	−207	40	−175
 3-Ethyl-2-pentene	4.4×10^{-5}	1.5×10^{-3}	35	42	−210	39	−189
 4-Methyl-2-hexene	6.8×10^{-5}	9.6×10^{-4}	14	40	−212	10	−276
 2-Octene	3.0×10^{-3}	3.0×10^{-2}	10	28	−215	7	−257
 1-Phenyl-propene	2.8×10^{-3}	2.0×10^{-2}	7	29	−213	8	−256

^a Ref. [27].

^b Ratio of TOFs: TOF of the imprinted Rh dimer catalyst (26)/TOF of the supported catalyst (24).

^c E_a : kJ mol⁻¹.

^d $\Delta^\ddagger S$: J K⁻¹ mol⁻¹.

and geometric effects of the ligands. There is a large decrease between 3-ethyl-2-pentene and 4-methyl-2-hexene (4-ethyl-2-pentene) due to the difference in the shape of the alkenes. The difference in the TOF ratios between 4-methyl-2-pentene and 4-methyl-2-hexene is also large, where the difference in the size of a methyl group is discriminated on the species (26). Thus, the molecular imprinting catalyst discriminates the size and shape of the alkenes.

After the imprinting, significant differences between small and large alkenes were observed in both activation energies and activation entropies. The activation energies for the hydrogenation of 3-ethyl-2-pentene and smaller alkenes on the species (26) were 26–43 kJ mol⁻¹, which are similar to the values observed on the species (24). In contrast, for the larger alkenes such as 4-methyl-2-hexene, 2-octene, and 1-phenylpropene, the activation energies were 10, 7, and 8 kJ mol⁻¹, respectively, which are small compared with those for the species (24) and other metal complex catalysts. Furthermore, the activation entropies reduced significantly from about −210 J mol⁻¹ K⁻¹ to about −260 J mol⁻¹ K⁻¹. The conspicuous change in the kinetic parameters for the larger alkenes parallels the change in enhancement of the reaction rates. These dramatic decreases in the activation energy and the TOF ratio can be explained by shift of the rate-determining step from the alkyl formation to the coordination of alkene to the Rh site regulated by wall of the cavity and remaining P(OCH₃)₃ ligands. For the alkenes with

the larger sizes and different shapes compared to the template, coordination to the Rh site through the cavity space becomes rate determining in the reaction sequences. The location of the Rh center to which the alkenes coordinate, the conformation of remaining P(OCH₃)₃ ligand, the orientation of template vacant site on Rh, the template cavity shape, the architecture of the cavity wall, and the micropore surrounding the Rh dimer in the SiO₂-matrix overlayers provide active reaction space (26) for size- and shape-selective hydrogenation of the alkenes [27].

The regulation of simple alkenes without any functional groups is generally difficult. Metal-complex coordination, unsaturation of the metal center, template-shaped cavity, and the architecture of surface matrix overlayers integrate to regulate the catalysis at the surface. The method combining metal-complex attachment and molecular imprinting on the surface demonstrates that the strategy can regulate and design chemical reactions at a molecular level such as with artificial enzyme catalysts.

6. Summary

Unique catalytic properties of metal complexes, which are very different from those of metal and metal oxides, have been applied to selective oxidation catalysis, shape selective catalysis, asymmetric catalysis, etc. Attaching metal complexes on oxide surfaces, followed by chemical events such as ligand

exchange, structural transformation, etc. on the surfaces, provides new catalytic systems with the advantageous properties of both heterogeneous and homogeneous catalysts. The fine regulation of the coordination sphere of the supported metal complexes and the reaction space on the active metal centers produce advanced catalytic materials toward perfect selectivity that ill-defined conventional catalysts are hard to achieve.

References

- [1] Y. Iwasawa, Tailored Metal Catalysts, D. Reidel, Dordrecht, 1986.
- [2] F.R. Hartley, Supported Metal Complexes, D. Reidel, Dordrecht, 1985.
- [3] Y. Iwasawa, Acc. Chem. Res. 30 (1997) 103.
- [4] A. Corma, H. Garcia, Adv. Synth. Catal. 348 (2006) 1391.
- [5] J.M. Thomas, R. Raja, D.W. Lewis, Angew. Chem. Int. Ed. 44 (2005) 6456.
- [6] J.M. Notestein, A. Katz, Chem. Eur. J. 12 (2006) 3954.
- [7] P. McMorn, G.J. Hutchings, Chem. Soc. Rev. 33 (2004) 108.
- [8] R.A. Sheldon, M. Wallau, I.W.C.E. Arends, U. Schuchardt, Acc. Chem. Res. 31 (1998) 485.
- [9] C. Coperet, J.M. Basset, Adv. Synth. Catal. 349 (2007) 78.
- [10] J.C. Fierro-Gonzalez, S. Kuba, Y.L. Hao, B.C. Gates, J. Phys. Chem. B 110 (2006) 13326.
- [11] M. Tada, Y. Iwasawa, Chem. Commun. (2006) 2833.
- [12] B.M.L. Dooos, I.F.J. Bankelecom, P.A. Jacobs, Adv. Synth. Catal. 348 (2006) 1413.
- [13] S. Kobayashi, R. Akiyama, Chem. Commun. (2003) 449.
- [14] K. Kaneda, K. Mori, T. Mizugaki, K. Ebitani, Curr. Org. Chem. 10 (2006) 241.
- [15] J.M. Thomas, W.J. Thomas, Principles and Practice of Heterogeneous Catalysis, VCH Weinheim, 1997.
- [16] M. Tada, Y. Iwasawa, Annu. Rev. Mater. Res. 35 (2005) 397.
- [17] M. Heitbaum, F. Glorius, I. Escher, Angew. Chem. Int. Ed. 45 (2006) 4732.
- [18] M. Tada, M. Shimamoto, T. Sasaki, Y. Iwasawa, Chem. Commun. (2004) 2562.
- [19] K. Asakura, K.K. Bando, Y. Iwasawa, H. Arakawa, K. Isobe, J. Am. Chem. Soc. 112 (1990) 9096.
- [20] M. Tada, T. Taniike, L.M. Kantam, Y. Iwasawa, Chem. Commun. (2004) 2542.
- [21] M. Tada, R. Coquet, J. Yoshida, M. Kinoshita, Y. Iwasawa, Angew. Chem. Int. Ed., in press.
- [22] M. Tada, N. Kojima, Y. Izumi, T. Taniike, Y. Iwasawa, J. Phys. Chem. B 109 (2005) 9905.
- [23] M. Tada, S. Tanaka, Y. Iwasawa, Chem. Lett. 34 (2005) 1362.
- [24] S. Tanaka, M. Tada, Y. Iwasawa, J. Catal. 245 (2007) 173.
- [25] M. Tada, Y. Iwasawa, J. Mol. Catal. A: Chem. 199 (2003) 115.
- [26] M. Tada, T. Sasaki, T. Shido, Y. Iwasawa, Phys. Chem. Chem. Phys. 4 (2002) 5899.
- [27] M. Tada, T. Sasaki, Y. Iwasawa, J. Catal. 211 (2002) 496.
- [28] M. Tada, T. Sasaki, Y. Iwasawa, Phys. Chem. Chem. Phys. 4 (2002) 4561.
- [29] M. Tada, T. Sasaki, Y. Iwasawa, J. Phys. Chem. B 198 (2004) 2918.
- [30] R. Bal, M. Tada, T. Sasaki, Y. Iwasawa, Angew. Chem. Int. Ed. 45 (2006) 448.
- [31] M. Tada, R. Bal, Y. Iwasawa, Catal. Today 117 (2006) 171.
- [32] K.K. Bando, K. Asakura, H. Arakawa, K. Isobe, Y. Iwasawa, J. Phys. Chem. 100 (1996) 13636.
- [33] M.D. Jones, R. Raja, J.M. Thomas, B.F.G. Johnson, D.W. Lewis, J. Rouzaud, K.D.M. Harris, Angew. Chem. Int. Ed. 42 (2003) 4326.
- [34] J.M. Thomas, R. Raja, D.W. Lewis, Angew. Chem. Int. Ed. 44 (2005) 2562.
- [35] J.M. Fraile, J.I. Garcia, J.A. Mayoral, M. Roldan, Org. Lett. 9 (2007) 731.
- [36] P. O'Leary, N.P. Krosveld, K.P. De Jong, G. van Koten, R.J.M.K. Gebbink, Tetrahedron Lett. 45 (2004) 3177.
- [37] S.S. Eaton, K.M. More, B.M. Sawant, G.R. Eaton, J. Am. Chem. Soc. 105 (1983) 6560.
- [38] D. Rehder, C. Schulzke, H. Dan, C. Meinke, J. Hanss, M. Eppe, J. Inorg. Biochem. 80 (2000) 115.
- [39] C.Y. Chu, D.R. Hwang, S.K. Wang, B.J. Uang, Chem. Commun. (2001) 980.
- [40] S.W. Hon, C.H. Li, J.H. Kuo, N.B. Barhate, Y.H. Liu, Y. Wang, C.T. Chen, Org. Lett. 3 (2001) 869.
- [41] Z. Luo, Q. Liu, L. Gong, X. Cui, A. Mi, Y. Jiang, Angew. Chem. Int. Ed. 41 (2002) 4532.
- [42] H. Somei, Y. Asano, T. Yoshida, S. Takizawa, H. Yamataka, H. Sasaki, Tetrahedron Lett. 45 (2004) 1841.
- [43] C.C. Romao, F.E. Kuhn, W.A. Herrmann, Chem. Rev. 97 (1997) 3197.
- [44] J. Okal, J. Baran, J. Catal. 203 (2001) 466.
- [45] D. Mandelli, M.C.A. van Vliet, U. Arnold, R.A. Sheldon, U. Schuchardt, J. Mol. Catal. A: Chem. 168 (2001) 165.
- [46] A. Salameh, C. Coperet, J.M. Basset, V.P.W. Bohm, M. Roper, Adv. Synth. Catal. 349 (2007) 238.
- [47] H.C. Lo, H.N. Han, L.J. D'Souza, S.C. Sinha, E. Keinan, J. Am. Chem. Soc. 129 (2007) 1246.
- [48] M. Onaka, T. Oikawa, Chem. Lett. 8 (2002) 850.
- [49] Y. Yuan, T. Shido, Y. Iwasawa, Chem. Commun. (2000) 1421.
- [50] Y. Yuan, Y. Iwasawa, J. Phys. Chem. B 106 (2002) 4441.
- [51] N. Viswanadham, T. Shido, Y. Iwasawa, Appl. Catal. A: Gen. 219 (2001) 223.
- [52] N. Viswanadham, T. Shido, T. Sasaki, Y. Iwasawa, J. Phys. Chem. B 106 (2002) 10955.
- [53] H. Liu, H. Imoto, T. Shido, Y. Iwasawa, J. Catal. 200 (2001) 69.
- [54] A. Katz, M.E. Davis, Nature 403 (2000) 286.
- [55] P.A. Brady, J.K.M. Sanders, Chem. Soc. Rev. 26 (1997) 327.
- [56] D.C. Sherrington, Chem. Commun. (1998) 2275.
- [57] M.E. Davis, A. Katz, W.R. Ahmad, Chem. Mater. 8 (1996) 1820.
- [58] B. Shellergren, Angew. Chem. Int. Ed. 39 (2000) 1031.
- [59] M.J. Whitecombe, C. Alexander, E.N. Vulfsen, Synlett 6 (2000) 911.
- [60] K. Mosbach, Chem. Rev. 100 (2000) 2495.
- [61] J.D. Marty, M. Mauzac, Adv. Poly. Sci. 172 (2005) 1.
- [62] J.J. Becker, M.R. Gagne, Acc. Chem. Res. 37 (2004) 798.
- [63] K. Morihara, M. Kurosawa, Y. Kamata, T. Shimada, J. Chem. Soc., Chem. Commun. 358 (1992).
- [64] J. Heilmann, W.F. Maier, Angew. Chem. Int. Ed. Engl. 33 (1994) 471.
- [65] A.G. Strikovskiy, D. Kasper, M. Crun, B.S. Green, J. Hradil, G. Wulff, J. Am. Chem. Soc. 121 (1999) 6640.
- [66] M.A. Markowitz, P.R. Kust, G. Deng, P.E. Schoen, J.S. Dordick, D.S. Clark, B.P. Gaber, Langmuir 16 (2000) 1759.
- [67] T. Tanimura, N. Katada, M. Niwa, Langmuir 16 (2000) 3858.
- [68] Y. Fujii, K. Matsutani, K. Kikuchi, J. Chem. Soc. Chem. Commun. (1985) 415.
- [69] J. Suh, Y. Cho, K.J. Lee, J. Am. Chem. Soc. 113 (1991) 4198.
- [70] J.F. Krebs, A.S. Borovik, J. Am. Chem. Soc. 117 (1995) 10593.
- [71] N.M. Brunkan, M.R. Gagne, J. Am. Chem. Soc. 122 (2000) 6217.
- [72] J. Matsui, I.A. Nicholls, I. Karube, K. Mosbach, J. Org. Chem. 61 (1996) 5414.
- [73] F. Locatelli, P. Gamez, M. Lemaire, J. Mol. Catal. A: Chem. 135 (1998) 89.
- [74] B.P. Santora, A.O. Larsen, M.R. Gagne, Organometallics 17 (1998) 3138.
- [75] K. Polborn, K. Severin, Chem. Eur. J. 6 (2000) 4604.
- [76] A.N. Cammidge, N.J. Baines, R.K. Bellingham, Chem. Commun. (2001) 2588.
- [77] Z.H. Meng, T. Yamazaki, K. Sode, Biotech. Lett. 25 (2003) 1075.
- [78] E. Burri, M. Ohm, C. Daguene, K. Severin, Chem. Eur. J. 11 (2005) 5055.
- [79] E. Burri, K. Severin, Chimia 60 (2006) 182.